A model realization of self-organized criticality for plasma confinement

B. A. Carreras, D. Newman, and V. E. Lynch
Oak Ridge National Laboratory, Oak Ridge, Tennessee 37831-8070

P. H. Diamond
University of California, San Diego, La Jolla, California 92093-0319

A model for plasma transport near marginal stability is presented. The model is based on subcritical resistive pressure-gradient-driven turbulence. Three-dimensional nonlinear calculations based on this model show effective transport for subcritical mean profiles. This model exhibits some of the characteristic properties of self-organized criticality. Perturbative transport techniques are used to elucidate the transport properties. Propagation of positive and negative pulses is studied. The observed results suggest a possible explanation of the apparent nonlocal effects observed with perturbative experiments in tokamaks. © *1996 American Institute of Physics.* [S1070-664X(96)03108-4]

I. INTRODUCTION

Many systems in nature are self-similar over extended ranges of spatial and temporal scales. In those systems, scale spectra may be described by power laws, and time spectra resemble the $1/f$-like distributions. Bak, Tang, and Wiesenfeld[1] suggested that there may be an intimate connection between the scale invariance in space and time, as is the case at critical transitions. Because there is no externally controlled critical parameter in natural systems, they call this basic property self-organized criticality (SOC). A running sand pile has been used as a simple dynamic system that exhibits these general properties.[2–4] Many models of natural phenomena like earthquakes,[5] forest fires,[6] and coevolution of biological species[7] satisfy the basic hypothesis of SOC.

Here, we are interested in the particular case of the transport processes in magnetically confined plasmas. These processes seem to have some of the characteristic properties of SOC systems. For instance:

(1) Since the proposal of the profile consistency principle,[8] the resilience of plasma profiles has been adopted in many transport models in a variety of formulations. This concept suggests that the existence of a critical gradient, or a gradient scale length, plays an important role in confinement.

(2) In the low-confinement (L-mode) regime, the energy-confinement time scales with the minor radius of the device. That is, transport scaling is Bohm-like.[9] However, the core fluctuation correlation length is of the order of a few ion Larmor radii.[10] These experimental results suggest the importance of interaction of disparate length scales in L-mode transport.

(3) The broad-band fluctuation spectrum in Ohmic and L-mode discharges has a frequency dependence that is not very sensitive to changes in global parameters. The spectral decay is often close to $1/f$.[11]

(4) A common result of stability analysis is that experimentally measured plasma profiles are found to be close to marginal ballooning stability.[12] This finding led to L-mode transport models based on marginal stability to ideal ballooning modes.[13]

Because of these properties, SOC has been proposed as a paradigm for understanding plasma profile dynamics.[14,15] Up to now, the paradigm used for the tokamak transport application of the SOC concept has been based on the sand pile analog. For numerical calculations,[15] a cellular automaton has been used, and for the analytical studies, a nonlinear Burgers equation[14] has been examined. It should also be noted that the situation studied here is closer to a hydrodynamic SOC with overlapping avalanches than to a SOC with vanishing weak drive. Near the threshold of avalanche overlap, the SOC dynamics closely resemble those of a percolation cluster slightly above criticality. Hence, hydrodynamic models, which are motivated by analogy to fully developed turbulence, are not applicable to the near threshold of avalanche overlap.

Here, we develop a model that contains some of the basic properties of plasma turbulence without bringing in all the complex details of the toroidal confinement device. This approach will allow us to explore the interplay of fluctuations and transport in a simple model realization of a plasma near marginal stability. This model is found to have some of the characteristic properties of a SOC system. In the numerical calculation presented, we have reduced the separation of time scales characteristic of a physical experiment that makes numerical calculations involving both fluctuations and transport time scales prohibitive.

The basic turbulence model is introduced in Sec. II, with the relaxation to a submarginal steady state discussed in Sec. III. The dynamical evolution of the model leading to subcritical transport is discussed in Sec. IV. The transport properties of the model are further explored by perturbative transport studies in Sec. V. These studies suggest a possible scenario to explain some of the anomalous observations when cold pulse perturbations are triggered at the tokamak edge. In Sec. VI, general ideas to experimentally test models based on the SOC concept are put forward, and finally, in Sec. VII, the conclusions of the paper are presented.

II. TURBULENCE MODEL

We start with a cylindrical plasma confined by a magnetic field with average bad curvature. This plasma can be unstable to resistive interchange modes. The dissipative terms control the instability threshold. A typical example of this type of plasma is the outer region of sheared stellarator devices. In the past, the resistive pressure-gradient-driven turbulence has been used to describe these plasmas in a supercritical state.[16] Now we use the same basic model to study a subcritical state. In this model, the fluctuation equations are the same as those discussed in Ref. 16,

$$\frac{\partial \nabla_\perp^2 \tilde{\Phi}}{\partial t} + \langle V_\theta \rangle \frac{1}{r} \frac{\partial \nabla_\perp^2 \tilde{\Phi}}{\partial \theta} + \tilde{\mathbf{V}} \cdot \boldsymbol{\nabla} \nabla_\perp^2 \tilde{\Phi}$$

$$= -\frac{1}{\eta m_i n_0 R_0} \nabla_\parallel^2 \tilde{\Phi} + \frac{B_0}{m_i n_0} \frac{1}{r_c} \frac{1}{r} \frac{\partial \tilde{p}}{\partial \theta} + \mu \nabla_\perp^4 \tilde{\Phi}, \qquad (1)$$

$$\frac{\partial \tilde{p}}{\partial t} + \langle V_\theta \rangle \frac{1}{r} \frac{\partial \tilde{p}}{\partial \theta} + \tilde{\mathbf{V}} \cdot \boldsymbol{\nabla} \tilde{p} = \frac{\partial \langle p \rangle}{\partial r} \frac{1}{r} \frac{\partial \tilde{\Phi}}{\partial \theta} + \chi_\perp \nabla_\perp^2 \tilde{p} + \chi_\parallel \nabla_\parallel^2 \tilde{p}. \qquad (2)$$

Here, p and Φ are the pressure and electrostatic potential, the tildes indicate fluctuating quantities (in time and space), and the angular brackets, $\langle \, \rangle$, indicate flux surface averaging, that is the poloidal and toroidal angular average. The toroidal magnetic field is B_0, the ion mass is m_i the averaged radius of curvature of the magnetic field lines is r_c, and the resistivity is η. The total flow velocity is expressed in terms of an averaged poloidal velocity plus a fluctuating component given in terms of a streamfunction $\tilde{\Phi}/B_0$,

$$\mathbf{V} = \langle V_\theta \rangle \hat{\theta} + (\boldsymbol{\nabla} \tilde{\Phi} \times \hat{z})/B_0, \qquad (3)$$

where $\langle V_\theta \rangle$ is the poloidal flow velocity, which is a function only of t and r, and $\hat{\theta}$ and $\hat{z}$ are unit vectors in the poloidal and toroidal directions, respectively. The velocity stream function $\tilde{\Phi}/B_0$ is trivially related to the electrostatic potential $-\tilde{\Phi}$. In both Eqs. (1) and (2), there is a dissipative term with the characteristic coefficients μ (the collisional viscosity) and $\chi_\perp$ (the collisional cross-field transport), respectively. A parallel dissipation term is also included in the pressure equation. This term can be interpreted as the parallel thermal diffusivity.

The instability drive is the flux surface averaged pressure gradient, $\partial \langle p \rangle / \partial r$, which is a function of r and t. A main difference between the model in Ref. 16 and the one considered here is in the evolution of the flux surface averaged quantities. The evolution equation of the flux surface averaged pressure is

$$\frac{\partial \langle p \rangle}{\partial t} + \frac{1}{r} \frac{\partial}{\partial r} r \langle \tilde{V}_r \tilde{p} \rangle = S_0 + S_1 + D \frac{1}{r} \frac{\partial}{\partial r} \left(r \frac{\partial \langle p \rangle}{\partial r} \right). \qquad (4)$$

It contains a time independent source term, S_0, which is only a function of r. This source of particles and heat is due, for instance, to neutral beam heating and fueling. In this case, S_0 is essentially determined by the beam deposition profile. Even the best beams have time and radial variations in the amount of heat deposited, this is represented by an added noise term, S_1, which we choose to be random in radius and time. Implicitly, S_1 reflects variations on time scales slower

than fluctuation time scales, hence its poloidal isotropy. The surface averaged quantities are not static, but vary on time scales long compared to the fluctuations. We will discuss below the sources of noise in this system and their meanings. The collisional diffusion coefficient, D, is taken to be different from the one in the fluctuation equation, Eq. (2).

We assume that away from marginal stability there is a steady state solution, $p_{eq}(r)$, for which the source term is identically cancelled by the radial diffusion. The evolution equation of the averaged pressure is

$$\frac{\partial (\langle p \rangle - p_{eq})}{\partial t} + \frac{1}{r} \frac{\partial}{\partial r} r \langle \tilde{V}_r \tilde{p} \rangle$$

$$= S_1 + D_0 \frac{1}{r} \frac{\partial}{\partial r} \left(r \frac{\partial (\langle p \rangle - p_{eq})}{\partial r} \right). \qquad (5)$$

The main transport mechanism that we study is the turbulent transport through the second term in the left-hand side of Eq. (5). However, the collisional diffusion term on the right-hand side is not is negligibly small for the calculations presented in this paper.

The coupling of the fluctuations to the averaged radial electric field is taken into account only through the poloidal velocity contribution. The time evolution of the latter is given by

$$\frac{\partial \langle V_\theta \rangle}{\partial t} = -\frac{1}{r^2} \frac{\partial}{\partial r} (r^2 \langle \tilde{V}_r \tilde{V}_\theta \rangle) - \hat{\mu} \langle V_\theta \rangle$$

$$= \langle \tilde{V}_r \nabla_\perp^2 \tilde{\Phi} \rangle - \hat{\mu} \langle V_\theta \rangle. \qquad (6)$$

Here, $\hat{\mu}$ is the flow damping caused by the magnetic pumping. The nonlinear convection terms in the poloidal momentum balance generate the nondiagonal $r\theta$ terms of the Reynolds stress tensor, which can be interpreted as a turbulent vorticity flux.

To reach to a self-organized state (when such a state exists), it is very important for noise to exist in the system. In some simple dynamical models, like the sand pile, the noise is external noise and the SOC state is reached by taking the limit of small noise. Therefore, it is difficult to prove the existence of such SOC states in problems that are solved numerically. It is even more difficult in a complex problem like the one presented here. In the model presented here, there are three types of noise:

(1) To start the three-dimensional nonlinear calculations, a low level of background fluctuations are initialized. These are the seeds for the instabilities to grow. We chose a random distribution of amplitudes and phases with an averaged fluctuation level below 10^{-5}. In our experience, for fluctuation levels this low, the results in the nonlinear regime are not sensitive to these initial conditions, although this is very difficult to prove without a study of many realizations. Systematic studies of the initial conditions for these equations have only been done for two-dimensional turbulence.[17]

(2) There is the noise associated with the fluctuations as the resistive interchange at different radial positions become unstable. The fluctuations evolution is given by Eqs. (1) and (2), and they induce transport of the averaged pressure and

flow through the nonlinear fluxes in Eqs. (5) and (6) and generate flow through the Reynolds stress term in Eq. (6).

(3) The third source of noise is the external pressure source in Eq. (5). Since this model has intrinsic noise because of the fluctuations, the external noise is not necessarily needed to reach an SOC state. A continuum source could lead to essentially the same results. There are several reasons to introduce a noise source. First, it is useful in comparing with the sand pile analog of the transport. A second reason is that the noise source allows one to separate the transport events and visualize the different scale length of these events. As the noise becomes more continuous, the transport events overlap and it is difficult to characterize them. In practice, all thermal and particle sources are noisy, therefore, such source terms are not unrealistic.

Numerical calculations show that the time averaged steady-state profile is essentially the same with or without the external noise source. Therefore, for the dynamical model including fluctuations to be close to an SOC state, such a source is not required. Tests of the results for different types of sources have been done. The tests are limited to a few cases due to the expense of these calculations. The results are not sensitive, as is shown below.

III. EQUILIBRIUM SOLUTION NEAR MARGINAL STABILITY

To investigate the transport dynamics close to marginal stability, the model must have a critical pressure gradient below which resistive interchange modes are stable. This is achieved by having finite values of the dissipative terms in the fluctuation equations. Here, we take $\mu = 0.2\ a^2/\tau_R$ and $\chi_\perp = 0.05\ a^2 \tau_R$, where $\tau_R \equiv a^2\ \mu_0/\eta$ is the resistive time and a is the minor radius. The parallel thermal diffusivity is $\chi_\parallel = 10^5\ R^2/\tau_R$. The resistivity is such that the Lundquist number is $S = 10^5$ for all these calculations and $\beta_0/2\epsilon^2 = 0.018$.

First, we consider the evolution of the system without average poloidal velocity. This constitutes the simplest form of the model. We start with a pressure profile well above the critical profile. To avoid problems with the boundaries, only modes with resonant surfaces in the range $0.2 > r/a > 0.8$ have been included in the calculation. We include 220 Fourier components for the calculations without flow and 440 for those with flow. The radial grid resolution is $\Delta r = 7.5 \times 10^{-4}$ a. The number of modes included in these calculations is low compared with the number we have included in studies of developed supercritical turbulence. However, in this model, transport is dominated by the profile relaxation processes. Therefore, we do not expect that a broad spectrum of modes is needed on each flux surface. The nonlinear evolution has been carried out with the KITE[18] code.

The system has been allowed to evolve to a stable state. The source term has been set to zero in the pressure equation to allow the relaxation to a stable state. To reach a SOC state, a very low value of the average pressure diffusivity is required. Otherwise, a slow diffusion of the averaged pressure smoothes the nonlinear modification of the average profile and sustains the instability. This effect is illustrated in Fig. 1, where the time evolution of the electrostatic potential fluc-
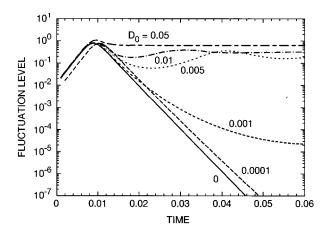

FIG. 1. Time evolution of the electrostatic potential fluctuation for different values of the collisional diffusivity of the averaged pressure, D_0.

tuation is plotted versus the time for different values of D_0. For $D_0 = 0$, the fluctuations decay with a decay rate comparable to the instability growth rate. To have a proper representation of this time scale, we need $D_0 < 0.001\ a^2/\tau_R$. In practice, for a full three-dimensional nonlinear calculation, it is not possible to have $D_0 = 0$, for numerical reasons. Therefore, we have used $D_0 = 0.0001\ a^2/\tau_R$ in all the calculations presented here.

When all perturbations have decayed and the pressure profile has relaxed (Fig. 2), the system is in a steady state. We will see that this state has the typical properties of the SOC state. First, note that this system is *not* marginally stable; it is more stable than marginal. This fact is clear from the nonlinear evolution of a single helicity. In Fig. 1, we have plotted the time evolution of the rms potential fluctuation level for different values of D_0. The linear growth rate is unaffected by D_0; hence, all m's grow at the same rate. At about $t = 0.008\tau_R$, the evolution enters the nonlinear phase and the instability saturates. At the same time, the nonlinear modification of the pressure profile reduces the instability drive. For $D_0 = 0$, the fluctuation level decays very fast after reaching the nonlinear state. In this case, the pressure gradient in the nonlinear state is well below the critical gradient, and the mode is stabilized. Therefore, the nonlinear evolution
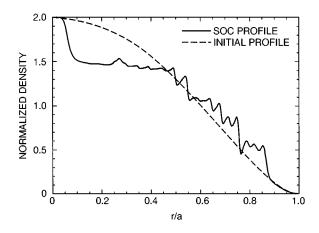

FIG. 2. For $D_0 = 0.0001\ a^2/\tau_R$ in Fig. 1, when all perturbations have decayed, the pressure profile relaxes to a SOC steady state.

has led the profile not to the marginal stable point, but rather well below. Indeed, the local gradient dynamics exhibit a sort of inertia which results in evolving past marginality to stability. As we increase D_0, the increased collisional diffusion smoothes the pressure profile, and the change in the gradient can lead to sustainment of the instability. These effects can be further studied by evaluating the linear stability of the final profile after nonlinear evolution. In the case of $D_0=0$, the stability calculation gives significantly negative growth rates. The fact that the resulting profile is more stable than marginal is a characteristic property of the SOC state,[15] although we cannot prove by just this observation alone that this state is a SOC state.

If we allow the poloidal velocity to evolve and the flow damping rate is low enough, there is a modification of the velocity profile induced by the Reynolds stress term. We can now repeat the relaxation process just described. In this case, the pressure profile after relaxation is different from the case without flow. The reason is the stabilizing effect of the poloidal velocity shear that changes the linear stability threshold and, as a consequence, changes the critical gradient. Therefore, the final pressure profile will depend on the averaged level of the poloidal velocity. Since this level is a function of the turbulence and closely related to it, the calculation including poloidal flow can not be broken into two steps. A full nonlinear calculation with sources is required each time.

IV. TRANSPORT PHENOMENA IN STEADY STATE

The next step in the development of the transport model is to consider the time evolution of the steady state with a noise source added. Here, the assumption is that, in a time-averaged sense, the equilibrium pressure source maintains the averaged gradient. However, this source is, in general, noisy. This noise is responsible for the dynamics in steady state. The noise is taken into account in the calculation as follows. At a fixed number of time steps (typically between 100 and 400), a small averaged pressure perturbation is added with a 50% probability. This perturbation is radially localized. It has a Gaussian form with a width of $W=0.01a$; the amplitude is 0.05 times the local value of the normalized (to its $r=0$ value) equilibrium pressure. The radial location of the averaged pressure perturbation is randomly chosen in the range $0.2>r/a>0.5$. The initial state is the stable relaxed pressure profile in Fig. 2. A very low random level of nonaxisymmetric perturbations is also initialized (about 0.001% fluctuations) as a seed for the instabilities. We consider first the case without averaged poloidal velocity.

As the average pressure perturbations are added, they trigger local instabilities in the plasma at the corresponding resonance surface. The instability locally flattens the pressure profile and causes a change of gradient in the nearby surfaces, which may become unstable and so continuing the process. Eventually, the excess pressure deposited at the core is transported to the edge of the plasma. This process has the characteristic properties of an avalanche.[1] It is a true avalanche in the sense that there is propagation both up and down the gradient. The downward propagation is dominant.

To quantify the global transport process, we evaluate the time evolution of the following quantities:
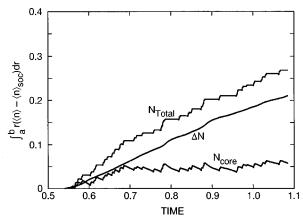

FIG. 3. Time evolution of the total pressure and the pressure in the core. The system reaches a steady state when N_{core} stays constant in time.

$$N_{core}=\int_0^{0.5a} r\,dr(\langle p\rangle-\langle p\rangle_{ss})$$

and

$$N_{Total}=\int_0^a n\,dr(\langle p\rangle-\langle p\rangle_{ss}). \tag{7}$$

Here, $\langle p\rangle_{ss}$ is the pressure profile obtained in the previous section by relaxing the initial pressure profile to steady state. In Fig. 3, we plotted N_{core}, N_{Total}, and $\Delta N=N_{Total}-N_{core}$. We can see that after a transition time, the system reaches a steady state in which N_{core} stays constant in time. That is, there is no accumulation of pressure at the core, and all added pressure is transported out. There is some accumulation in the outer region, $r/a>0.5$, because of the boundary conditions. That is the reason to look at the $r/a=0.5$ surface. The effective flux through the $r/a=0.5$ surface is equal to the rate of change of ΔN. Therefore, an incremental effective diffusivity can be defined by

$$D_{eff}\equiv\frac{\partial\Delta N}{\partial t}\bigg/ r\,\frac{\partial\langle p\rangle}{\partial r}\bigg|_{r=0.5a}. \tag{8}$$

Using the same data as in Fig. 3, we have plotted the effective diffusivity as a function of time in Fig. 4. This incremental effective diffusivity makes sense only as a time-averaged quantity. Note that the theoretical calculations produce a result only in the Markovian limit. Over the time range considered, its averaged value is $D_{eff}=0.076a^2/\tau_R$. This value is more than 2 orders of magnitude above D_0. Therefore, as is typical in SOC systems, there is effective transport in subcritical conditions. Note that this diffusion is only the incremental diffusion associated with the noise source. It is not the total diffusion needed in maintaining the equilibrium. This transport coefficient is a function of the "noise level." That is, transport regulates itself to remove the needed amount of pressure. To find the scaling with noise level is difficult because it takes a long time to perform these nonlinear calculations over the time scales required. We investigate the scaling by the use of pressure pulses.

The transport process has length scales that range from the individual single-mode width, W_k, to the full plasma minor radius. This can be seen in Fig. 5(a), where we have
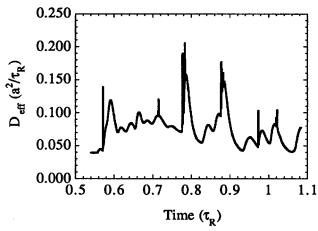
FIG. 4. For the case of Fig. 3, an effective diffusivity is defined from the flux through the $r/a=0.5$ surface, which is equal to the rate of change of ΔN.

plotted incremental averaged pressure, $\langle p \rangle - \langle p \rangle_{ss}$, contours as a function of the radial position and time ($r-t$ plane). It is easy to identify individual transport events (avalanches) triggered by the pressure drops. These avalanches involve the destabilization of several instabilities at different resonant surfaces. Each avalanche can be characterized by a length [see green contours in Fig. 5(a)]. The trajectories of the transport events in the $r-t$ plane clearly show that the propagation is not ballistic; it has an essentially diffusive character. In Fig. 5(b), we have plotted the rms level of fluctuation in the same $r-t$ plane. It is clear from this plot that the dominant scale length of the fluctuations is of the order of the mode width W_k. This is another property of this type of model: The radial correlation length of the flux is much longer than the fluctuation radial scale. Similarly, in the sand pile model, the fluctuation scale is identified with the basic cell size while the avalanches can reach the whole system size.[15]

Let us find the impact of these mixed scale lengths on the diffusion coefficient. We can calculate the time averaged flux and the averaged pressure profile in the steady state phase of the calculation (Fig. 6). It is interesting to notice that the averaged flux increases approximately linearly with radius, as in the case of the running sand pile.[15] The pressure profile shows all the structures of the order of a mode width. To calculate a diffusion coefficient, we fit both by a linear function of r and that gives us $D_{eff} \approx 0.33\ (r-r_0)$. In spite of the apparent diffusive character of the single transport event, the averaged diffusion coefficient has a radial scale dependence which is consistent with Bohm-type scaling. This result is in good agreement with the numerical sand pile results[15] and with the analytical calculations.[14]

There is also a broad range of time scales involved in the transport process. The best way to find the relevant time scales is to Fourier-analyze the local fluctuations. We analyze the time trace of the electrostatic potential fluctuations at a fixed spatial location. Because the diamagnetic rotation terms have not been included in this calculation, the fast oscillatory time scale is not present. Therefore, this time trace is equivalent to the envelope of the fluctuations trace. The analysis of these data leads to the results plotted in Fig.
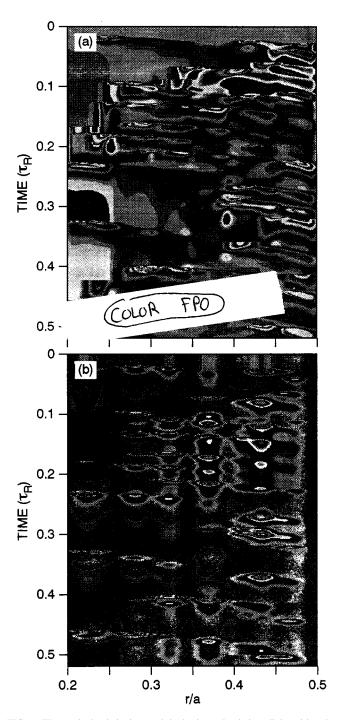

FIG. 5. The vertical axis is time and the horizontal axis is radial position. In this plane, we plot (a) averaged pressure contours and (b) rms potential fluctuation contours.

7. The fluctuation spectrum has three characteristic regions. In the very low frequency region, the spectrum is flat. For frequencies in the range $5 \times 10^{-4} \tau_{Hp}^{-1} < f < 10^{-2} \tau_{Hp}^{-1}$, the dependence of the spectrum on f is close to $1/f$. At higher frequencies, the spectrum falls off as f^{-4}. These three spectral regions have been identified in the sand pile model[4] and they are characteristic of many SOC systems.

To test the resilience of these results to the form of the external noise, we have repeated the calculation with the same form of the noise source but decreased the size of the
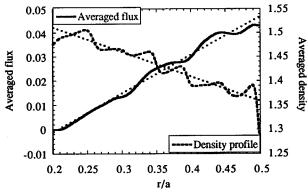
FIG. 6. Time-averaged flux and pressure gradient during the steady state phase for the calculation in Fig. 3.

FIG. 8. Propagation of a positive pulse from $r_0/a = 0.2$. In the $t-r$ plane, we have plotted averaged pressure contours.

pressure perturbations by a factor of 4 and increased their frequency by the same factor. In this way, the time integrated pressure source is the same. The result for the diffusivity does not change. The transport events have stronger overlap due to the increased frequency, but the average transport properties do not change.

The addition of poloidal flow makes this calculation considerably more complex as there is interplay between the shear flow and turbulence.[19] The shear flow is amplified by turbulence, and at the same time the shear flow regulates the turbulence level and the transport scales. This interplay is very important in the case of the pulse propagation discussed in the next section. Here, we want to emphasize a double role played by the shear flow. First, it changes the critical gradient, as has been discussed in the previous section. The second effect is the decorrelation of the turbulence and of the transport events. This second effect was studied in the sand pile model and with the Burgers equation, with the result of the modification of the basic scaling of the effective diffusivity. Because of the number of nonlinear calculations required to test this scaling, this study is beyond the scope of the present work.
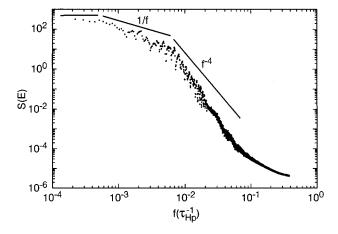
V. PULSE PROPAGATION STUDIES

Using the model developed in the previous sections, we have studied the propagation of pressure pulses in the plasma. Two types of pulses have been considered: positive pressure perturbations at the plasma center and negative pressure perturbations at the plasma edge.

Let us first consider a positive pressure pulse produced at the center of the plasma. An averaged pressure perturbation is produced at $r_0 = 0.2a$. We use a Gaussian form with a width of $0.02a$. For different values of the amplitude of the pulse, we follow its time evolution. In Fig. 8, we have plotted the contours of the averaged pressure perturbation in the $t-r$ plane, as was done in Fig. 5(a). The pulse propagation is very similar to the one for a single transport event plotted in Fig. 5. The time evolution of the averaged pressure pulse is shown in Fig. 9. The change of the waveforms with time is quite different from the results of simple diffusion, although the determination of the time scales will indicate diffusive propagation. To interpret in a quantitative way the evolution of the pulse, we use the same method that the experimentalists use for heat pulse propagation.[20] By evaluating the time delay, Δt, for the peak of the pulse to reach a given radial position r, we can plot Δt vs $(r-r_0)^2$. From this plot (Fig. 10), we see that the propagation is consistent with diffusive propagation, and we can derive an effective diffusivity. The

FIG. 7. The electrostatic potential fluctuation spectrum at $r/a = 0.35$, $\theta = \pi/4$, and $\zeta = 0$. This spectrum has the three characteristic regions observed in the sand pile model.
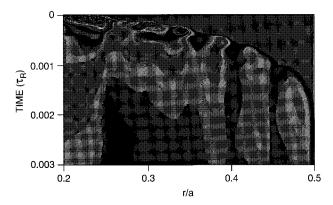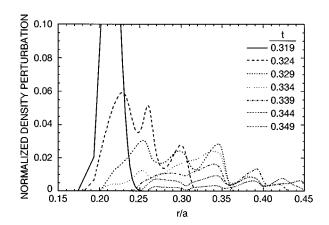

FIG. 9. Averaged pressure pulse at different times for the case shown in Fig. 7.

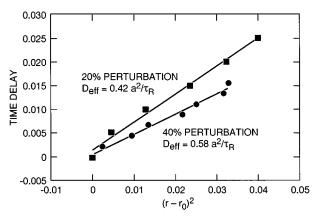FIG. 10. Time delay for the maximum of the pulse to reach the position r. Two cases with different amplitude of the initial pulse are plotted.

FIG. 12. Time of arrival of the leading edge of the negative pulse at a position r. The pulse moves inwards at approximately constant velocity.

calculated effective diffusivity is a function of the size of the pulse. Using different size pulses, we conclude that the dependence of the effective diffusivity with the amplitude of the pulse, P, is $D_{eff} \propto P^{0.45}$. This result is consistent with the analytical determination of the diffusivity based on the nonlinear Burgers equation.[14] However, this result also cautions us about identifying a process with diffusion on the basis of the analysis of Fig. 10.

If a negative pressure pulse is generated at the plasma edge, the propagation dynamics are quite different from the internal positive pulse. A typical example of negative pulse propagation is shown as a $t-r$ plot in Fig. 11. The perturbation is produced at $r_0 = 0.6a$ with a width of $0.02a$. We can see that the leading edge of the pulse does not curve as it moves inward, as would be expected if diffusion were the dominant process. The leading edge of the pulse moves inward at constant velocity (Fig. 12). The propagation is fast, $V_{pulse} = 8.34a/\tau_R$. The propagation of the negative pulse has some of the characteristic properties of a propagating front[21] for fast transitions. One of them is the large leading-edge velocity. In the cases considered here, the propagation velocity is approximately given by $V_{pulse} \approx \gamma W$, where γ is the supercritical instability growth rate due to the increase of the local gradient by the pulse and W a characteristic scale length of the instability. Without coupling to the averaged
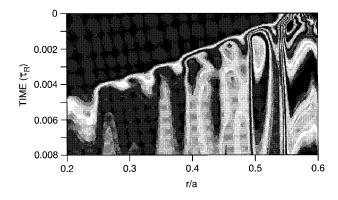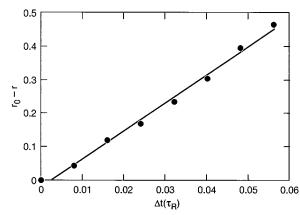
flow shear, the averaged negative pressure pulse propagates all the way through the plasma core.

When the self-consistent flow is coupled to the pulse evolution equation, shear flow is amplified. The level of shear flow depends on the turbulence level generated by the pulse and on the seed flow level. Because the latter is arbitrarily set, no definitive conclusion can be derived from this model. However, when the seed flow profile is above a threshold value, the generated shear flow can control the scale length in the problem. That is, the pulse does not penetrate all the way to the center of the plasma (Fig. 13). In Fig. 13, we plot the propagation of a negative pulse with parameters identical to those for the case of Fig. 11, but with averaged flow evolution and the noise source turned on. The propagation of the negative pressure pulse stops at $r/a \equiv 0.37$. At this point a transport barrier is formed, and confinement improves within $r/a \leqslant 0.37$. There is clear evidence of this effect because we have the noise source turned on and we can see pressure accumulation within this region (Fig. 14). This result is consistent with the transport bifurcation results from the analytical predictions[14] for SOC scaling with sheared flows.

The dependence of the resulting shear flow on the seed flow is one of the limitations of this model. The sheared electric field is the real parameter to include in this model to control the scale length of the propagation. This should incorporate the contribution of the gradient of the ion pressure. In this case, because we work with a finite pressure gradient, there is no ambiguous dependence on the seed for the electric field shear.

VI. EXPERIMENTAL TEST OF THE SOC MODELS

There are some general ideas in the SOC model for confinement that go beyond the limitations of the present model and could be experimentally tested. One of them is the concept of transport event, or avalanche-like transport. The transport events are not continuous but intermittent. This fact by itself is not a clear test of the model because the fluxes induced by supercritical turbulence also have intermittent character.[22] What is particular to SOC models is the difference between the characteristic scale lengths of the fluctuations and transport events. The high frequency range of the
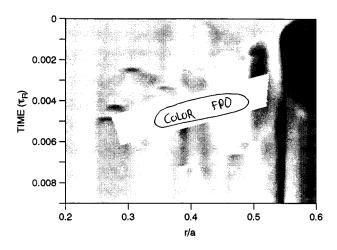

FIG. 11. Propagation of a negative pulse from $r_0/a = 0.6$. In the $t-r$ plane, we have plotted averaged pressure contours.

Phys. Plasmas, Vol. 3, No. 8, August 1996

Carreras et al.   2909

FIG. 13. Propagation of a negative pulse from $r_0/a=0.6$. In this case, there is coupling to a poloidal shear flow. The pulse stops at about $r/a=0.37$. In the $t-r$ plane, we have plotted the averaged pressure contours.

FIG. 15. Cross-correlation of the low frequency modulation at two radial positions peaks at a time delay corresponding to the propagation distance of the avalanche.

fluctuation spectrum decorrelates over the scale length of a mode width. However, the transport scale and the low modulation frequency of the fluctuation maintain a correlation over several mode widths. Furthermore, because transport events are avalanches, the coherence of the cross-correlation of the low frequency modulation at two radial positions peaks at a time delay corresponding to the propagation distance of the avalanche, $\Delta t \equiv (r-r_0)^2/D_{\text{eff}}$. This effect is shown in Fig. 15 for the calculation corresponding to Fig. 5. This long-range correlation with propagation of the very low frequencies offers a significant experimental test of the SOC transport mechanism. When an avalanche starts, there is a double propagation effect that can be interpreted as a bump moving down and a hole moving up the profile. The cross-correlation function has two maxima, one at positive Δt and another at negative Δt (Fig. 16).

A second property is the dependence of the diffusivity on the size of the pulse. This dependence is weak; it is a fractional power of the amplitude of the pulse. To test this effect, it is necessary to consider that small pulses will be below the threshold because of the background transport level. For large pulses, the effect of the radial electric field
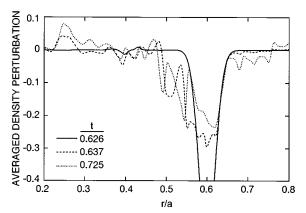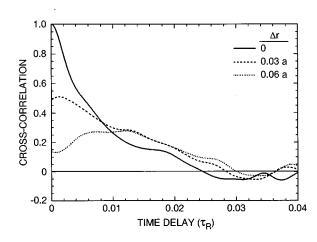
shear tends to weaken the dependence on the pulse amplitude. Therefore, it is difficult to define the range of pulse amplitudes where this dependence can be tested.[14]

The spectral decay index of the fluctuations has a rather universal value. This is a third property of these SOC models that could be explored experimentally. We do not have systematic information on the gross features of the fluctuation spectra in magnetically confined plasmas. A superficial look at published spectra suggests some kind of universal indexes for the broadband spectra. However, a systematic study is called for.

A fourth property that has experimental implications is the propagation of negative pressure pulses. In our simple model, this is the analog of the cold pulse propagation studied in different machines.[23,24] For several years, these experiments have been a serious puzzle. The propagation studies of the previous section suggest a possible scenario to explain these experiments. The cold pulses are created at the plasma edge; they propagate inward by triggering a sequence of local instabilities. The propagation is fast, and the leading edge of the pulse propagates with a constant velocity. With the triggering of the local instabilities, the sheared electric field, E_r', is amplified. When E_r' is large enough, it stops the in-
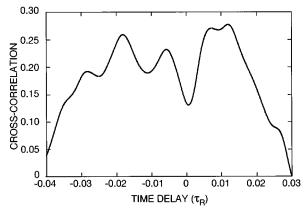

FIG. 14. Averaged pressure perturbation profiles for the case described in Fig. 12, showing the pulse stopping at $r/a=0.37$ and pressure accumulating inside the region $r/a<0.37$.

FIG. 16. Cross-correlation of the low frequency modulation at $r/a=0.35$. The cross-correlation has a double peak at $\pm\Delta t$, the time delay corresponding to the propagation distance of the avalanche.

Carreras *et al.*

ward propagation of the cold pulse. At the same time, the E'_r acts as a transport barrier, and the central plasma is better confined. The improved confinement leads to heating of the core. The experimental identification of a transport barrier associated with the propagation of these pulses could be a good test of this model.

VII. CONCLUSIONS

The model proposed in this paper has many of the characteristics of a SOC model, although it is not possible to rigorously prove that it is a SOC model. This is, of course, partially a consequence of the ambiguity which persists in the definition of SOC. This model is a very simplified form of turbulence for a magnetic confinement device, but it gives the main features of what can be expected if confinement is SOC. The transport properties put forward on the basis of a simple sand pile model[15] are well verified in this model that includes both fluctuations and transport. This is an indication that the main properties derived here do not depend on the particular underlying linear stability mechanism.

The time evolution of positive outward-propagating pulses can be described by a diffusive process, although the propagation is not pure diffusion. The effective diffusivity derived from the numerical calculations scales as a fractional power (approximately square root) of the amplitude of the pulse.

Inward-propagating negative pulses behave in a more complex way. The leading edge moves ballistically. With the propagating pulse there is E'_r amplification. The propagation depth of a cold pulse depends on the level of E'_r. The E'_r amplification by the pulse results in the formation of an internal transport barrier that causes the confinement improvement at the core. The barrier diffusively decays afterwards.

Many of the general features of the SOC model can be experimentally tested.

ACKNOWLEDGMENTS

[1] P. Bak, C. Tang, and K. Weisenfeld, Phys. Rev. Lett. **59**, 381 (1987).
[2] P. Bak, C. Tang, and K. Weisenfeld, Phys. Rev. A **38**, 364 (1988).
[3] L. P. Kadanoff, S. R. Nagel, L. Wu, and S. M. Zhou, Phys. Rev. A **39**, 6524 (1989).
[4] T. Hwa and M. Kadar, Phys. Rev. A **45**, 7002 (1992).
[5] B. E. Shaw, J. M. Carlson, and J. S. Langer, J. Geophys. Res. **97**, 479 (1992).
[6] B. Drossel and F. Schwabl, Phys. Rev. Lett. **69**, 1629 (1992).
[7] P. Bak and K. Sneppen, Phys. Rev. Lett. **71**, 4083 (1993).
[8] B. Coppi, Comments Plasma Phys. Controlled Fusion **5**, 261 (1980).
[9] F. W. Perkins, C. W. Barnes, D. W. Johnson, S. D. Scott, M. C. Zarnstorff, M. G. Bell, R. E. Bell, C. E. Bush, B. Grek, K. W. Hill, D. K. Mansfield, H. Park, A. T. Ramsey, J. Schivell, B. C. Stratton, and E. Synakowski, Phys. Fluids B **5**, 477 (1993).
[10] R. J. Fonck, N. Bretz, G. Cosby, R. Durst, E. Mazzucato, R. Nazikian, S. Paul, S. Scott, W. Tang, and M. Zarnstorff, Plasma Phys. Controlled Fusion **34**, 1993 (1992).
[11] A. J. Wootton, B. A. Carreras, H. Matsumoto, K. McGuire, W. A. Peebles, Ch. P. Ritz, P. W. Terry, and S. J. Zweben, Phys. Fluids B **2**, 2879 (1990).
[12] L. A. Charlton, D. K. Lee, R. M. Wieland, B. A. Carreras, W. A. Cooper, and G. H. Neilson, Nucl. Fusion **24**, 33 (1984).
[13] J. W. Connor, J. B. Taylor, and M. Turner, Nucl. Fusion **22**, 256 (1984).
[14] P. H. Diamond and T. S. Hahm, Phys. Plasmas **2**, 3640 (1995).
[15] D. E. Newman, B. A. Carreras, P. H. Diamond, and T. S. Hahm, Phys. Plasmas **3**, 1858 (1996).
[16] B. A. Carreras, L. Garcia, and P. H. Diamond, Phys. Fluids **30**, 1388 (1987).
[17] B. A. Carreras, V. E. Lynch, and L. Garcia, Phys. Fluids B **5**, 1795 (1993).
[18] L. Garcia, H. R. Hicks, B. A. Carreras, L. A. Charlton, and J. A. Holmes, J. Comput. Phys. **65**, 253 (1986).
[19] P. H. Diamond, V. Shapiro, V. Shevchenko, Y.-B. Kim, M. N. Rosenbluth, B. A. Carreras, K. Sidikman, V. E. Lynch, L. Garcia, P. W. Terry, and R. Z. Sagdeev, in *Proceedings of the Fourteenth International Conference on Plasma Physics and Controlled Nuclear Fusion Research* (International Atomic Energy Agency, Vienna, 1993), Vol. 2, p. 97.
[20] J. D. Bell, J. L. Dunlap, V. K. Paré, J. D. Callen, H. C. Howe, E. A. Lazarus, M. Murakami, and C. E. Thomas, Nucl. Fusion **24**, 997 (1984).
[21] P. H. Diamond, V. B. Lebedev, D. E. Newman, and B. A. Carreras, Phys. Plasmas **2**, 3685 (1995).
[22] B. A. Carreras, C. Hidalgo, E. Sánchez, M. A. Pedrosa, R. Balbín, I. García-Cortés, T. Estrada, B. van Milligen, D. E. Newman, V. E. Lynch, Phys. Plasmas **3**, 2664 (1996).
[23] K. Gentle, R. V. Bravenec, G. Cima, H. Gasquet, G. A. Hallock, P. E. Phillips, D. W. Ross, W. L. Rowan, A. J. Wootton, T. P. Crowley, J. Heard, A. Ourona, P. M. Schoch, and C. Watts, Phys. Plasmas **2**, 2292 (1995).
[24] M. W. Kissick, E. D. Fredrickson, and J. D. Callen, Bull. Am. Phys. Soc. **39**, 1678 (1994).